PHILOSOPHICAL TRANSACTIONS OF THE ROYAL SOCIETY A MATHEMATICAL, PHYSICAL & ENGINEERING SCIENCES

Three-Dimensional Mode Growth in Boundary Layers with Tuned and Detuned Subharmonic Resonance

T. C. Corke

Phil. Trans. R. Soc. Lond. A 1995 **352**, 453-471
doi: 10.1098/rsta.1995.0082

Three-dimensional mode growth in boundary layers with tuned and detuned subharmonic resonance

By T. C. Corke

Fluid Dynamics Research Center, Mechanical and Aerospace Engineering Department, Illinois Institute of Technology, Chicago, IL 60616, USA

This work involves the use of controlled periodic disturbances to excite a plane Tollmien–Schlichting (TS) wave at one frequency (f_{2D}) along with pairs of oblique waves with equal but opposite wave angles at a different frequency (f_{3D}) in order to study the resonant growth of 3D modes in a Blasius boundary layer. In our earlier work (Corke & Mangano 1989; Corke 1990), the frequency of the oblique modes was exactly the subharmonic of the plane Tollmien–Schlichting (TS) mode. These modes were also phase-speed locked so that in terms of their streamwise wave numbers, $\alpha_{2D} = \frac{1}{2}\alpha_{3D}$. This so-called 'tuned' subharmonic resonance leads to the enhanced growth of the otherwise linearly damped oblique waves, as well as the growth of higher harmonic 3D modes with frequencies and wave numbers: $(\frac{3}{2}f_{2D}, \frac{3}{2}\alpha_{2D}, \pm\beta_{3D})$, $(\frac{5}{2}f_{2D}, \frac{5}{2}\alpha_{2D}, \pm\beta_{3D})$, $(f_{2D}, \alpha_{2D}, \pm 2\beta_{3D})$ and $(0, 0, \pm 2\beta_{3D})$. Even when the initial 3D oblique waves have frequencies which are close to the TS subharmonic frequency, a 'detuned' subharmonic resonance leads to the enhanced growth of the 3D mode. In addition, it promotes the growth of numerous discrete modes produced by successive sum and difference interactions. These interacted modes are also three dimensional, with higher amplification rates that increase with the interaction order. The growth of these modes accounts for the rapid spectral filling, and low-frequency modulation commonly observed in natural subharmonic transition. Starting from a 'tuned' resonance, this scenario then provides a mechanism for the generation of a broad spectrum at the later stages of subharmonic mode transition. However, the results also suggest that with 'natural' transition, starting from low-amplitude broadband disturbances, the most likely 2D/3D resonance will be 'detuned'.

1. Background

It is now well established that the principle route to transition in a 2D boundary layer, having a linear growth regime, and in the absence of a strong adverse pressure gradient, is by a resonant interaction between a triad of modes made up of a plane Tollmien–Schlichting (TS) wave and pairs of oblique waves with equal–opposite wave angles. If all the modes are eigensolutions of the Orr–Sommerfeld equation, then the three-wave resonance is of a specific type first postulated by Craik (1971). Because this usually involves oblique modes at the subharmonic frequency of the plane mode, it is often referred to as subharmonic transition. Because it involves initially linear modes, it can occur at very-low initial amplitudes.

Phil. Trans. R. Soc. Lond. A (1995) **352**, 453–471
Printed in Great Britain

With slightly higher initial amplitudes, a different and more general mechanism for the first growth of three dimensionality comes into play. This was first presented by Herbert (1983). It involves the secondary instability of a basic flow made up of the mean flow and plane TS wave subject to spanwise periodic vorticity perturbations corresponding to Squire modes. This mechanism allows a spanwise wave-number selectivity based on amplification rate that is not present in Craik's approach.

The results of our early investigations (Corke & Mangano 1989; Corke 1990) have verified this wave-number selectivity as well as the eigenfunction structure of the principle and interacted modes up to and past the point of energy saturation. We have also shown that the process of transition in these cases is fundamentally different from that associated with earlier experiments, such as those performed by Klebanoff *et al.* (1962), which introduce a high (approximately 1% u'/U_∞) initial-amplitude plane TS wave. In those early experiments, the large TS forcing resulted in the development of an inflectional mean-velocity profile in a thin shear layer away from the wall in the outer part of the boundary layer. As a result of an inviscid instability, higher frequencies were produced which lead to a rather fast and violent 'breakdown' to turbulence.

In our cases, starting with low initial amplitudes (approximately 0.07% u'/U_∞) so that the initial modes pass through a linear growth stage, we did not observe strong inflections in the mean-velocity profile or high-frequency 'spike stages' associated with an inviscid instability. Rather, we observed a gradual spectral broadening at low, intermediate and higher frequencies. We have attributed this to a process of 'mode detuning', whereby the initially exact fundamental subharmonic interaction becomes gradually detuned, leading to the generation of frequency side bands. These side-band modes derive energy from the primary modes, and through sum and difference interactions produce new modes. Each successive generation of modes interacts with the others until the spectrum becomes relatively broadband. A bell-wether of this process is the appearance of a low-frequency component corresponding to the lowest difference mode. Such an increase in the energy in velocity fluctuations at low frequencies was observed in the experiments of Kachanov & Levchenko (1984). This was seen as a low-frequency amplitude modulation of the subharmonic mode. In their case they had only input a plane TS wave. The subharmonic mode that developed grew out of the background disturbances. They believed that the growth of the broad band of lower frequencies was due to stochastic modulation of the phase and amplitude of the subharmonic mode. In an effort to explain these observations, Santos & Herbert (1986) and Santos (1987) examined the secondary instability of the mean flow and fundamental TS wave to a 'detuned' subharmonic 3D perturbation. For this they found a broad peak of amplification which they felt could produce a similar type of low-frequency beating observed by Kachanov & Levchenko (1984). The width of the region of 'detuned' amplification was predicted to vary with amplitude and, in particular, broadened as the initial amplitudes increased.

Based on these observations, the left-hand side of figure 1 shows a scenario for reaching broadband velocity fluctuations associated with the transition to turbulence, starting from a subharmonic 3D mode resonance of the Craik or Herbert types. In this case, the pairs of oblique modes have a frequency and streamwise wave number which are exactly one-half those of the plane TS mode. As a result, the other travelling modes produced by sum and difference interactions are limited to intervals of the lowest difference frequency, $\frac{1}{2}f$, namely, f, $\frac{3}{2}f$, $2f$ and $\frac{5}{2}f$. The question in this process is how these few discrete modes develop into a broad spectrum of many modes, which we associate with a turbulent flow.

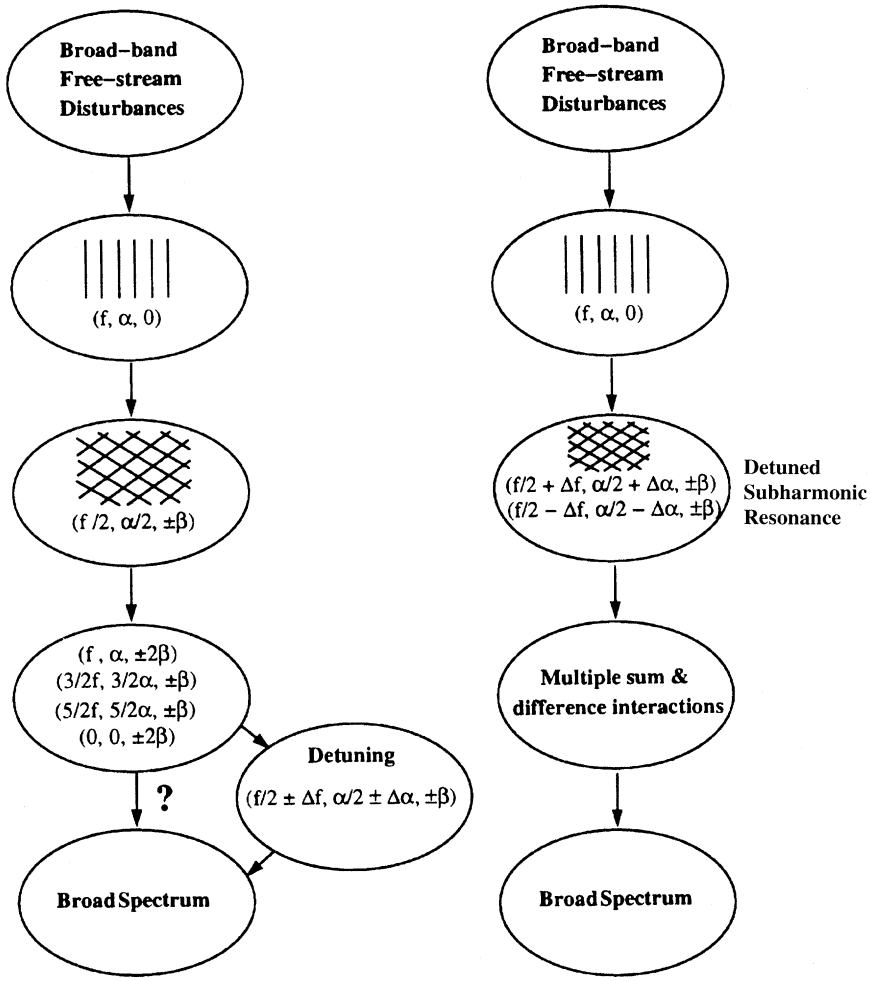

Figure 1. Schematic of two paths for the generation of a broadband spectrum of 3D modes starting from a 'tuned' (left) or 'detuned' subharmonic resonance.

Our attempt to answer this question is the motivation of the work described in this paper. The premise is that a 'detuning' of the initially 'tuned' subharmonic resonance is all that is needed to lead to the generation of a broad range of discrete modes. To study this in a controlled experiment, we start with conditions for a 2D/3D mode resonance which is initially 'detuned' from the exact fundamental/subharmonic frequencies used in our previous studies. The amount of frequency detuning and the initial amplitudes (2D and 3D) are parameters in this study. The results are contrasted with comparable 'tuned' resonance cases.

2. Experimental approach

As with our earlier experiments, we introduce both 2D and 3D disturbances into the boundary layer in order to seed simultaneously a plane TS wave and oblique wave pairs. This is achieved using a spanwise array of 0.05 mm diameter heating

Table 1. *Table of input conditions for* $U_\infty = 6.2$ m s^{-1}

case	$F_{2D} \times 10^6$	$F_{3D} \times 10^6$	θ/deg	F_{2D}/F_{3D}	% detuning
0	79	39.5	59	2.00	0.0
1	81	39.5	59	2.06	3.1
2	84	39.5	59	2.13	6.3
3	86	39.5	59	2.19	9.4
4	88	39.5	59	2.25	12.5

wires which are suspended at the height of the critical layer, at the streamwise location just upstream of the lower linear-stability neutral branch. A schematic drawing of the measurement section and heating wires is shown in figure 2. The wires are periodically heated to introduce controlled perturbations through local changes in the air viscosity. Each heating wire is individually controlled to allow a spanwise phase change between adjacent wires. Changing the phase allows different oblique wave angles. The plane wave is introduced using a separate single wire which spans the full width of the measurement section. This is located slightly upstream of the short-wire segments. The amplitude, frequency and phase of the periodic signal to the single (2D) wire are controlled separately from the (3D) wire segments. This allows us to independently change the initial conditions to the 2D and 3D disturbances. Further details of this method are contained in the paper by Corke & Mangano (1989).

To document both 'tuned' and 'detuned' fundamental/subharmonic resonance, we used oblique mode pairs with a spanwise wave number which matched the most amplified case of Corke & Mangano (1989). This corresponds to wave angles of 59°. The dimensionless frequency $F = 2\pi f\nu/U_\infty^2 \times 10^6$ for the oblique modes was also the same, $F = 39.5$.

The frequency of the oblique modes was kept fixed in the experiment. To study the effect of frequency detuning, the frequency of the plane wave was discretely varied from $79 \leqslant F \leqslant 88$. The lowest of these frequencies gives an exact 2:1 combination with the oblique modes. Table 1 summarizes the input conditions.

The conditions for the basic flow are the same as those documented by Corke & Mangano (1989). These correspond to a Blasius flow with a virtual origin located 45 cm upstream of the heating wire array.

The measurements consist of time series from a dual-sensor hot-wire designed to measure the streamwise U and spanwise W velocity components. The data series are acquired in phase with the input perturbation series so that the velocity fluctuations, which are related to the seeded instabilities, can be reconstructed in a phase-averaged sense in 3D space from a series of point measurements.

Measurements at only one spanwise z location are taken at an intersection of the opposite-angled oblique mode pairs, where the amplitude of the initial 3D mode in the spanwise direction is a local maximum. Otherwise, measurement points are taken as discrete locations in the wall normal y and spanwise directions at different streamwise x positions. Measurements at different spanwise locations are used to confirm the spanwise wavelengths of 3D modes. $x = 0$ corresponds to the location of the heating wire array. The boundary-layer virtual origin is at $x = -45$ cm. The region of streamwise locations brackets the upper branch of the linear-stability neutral

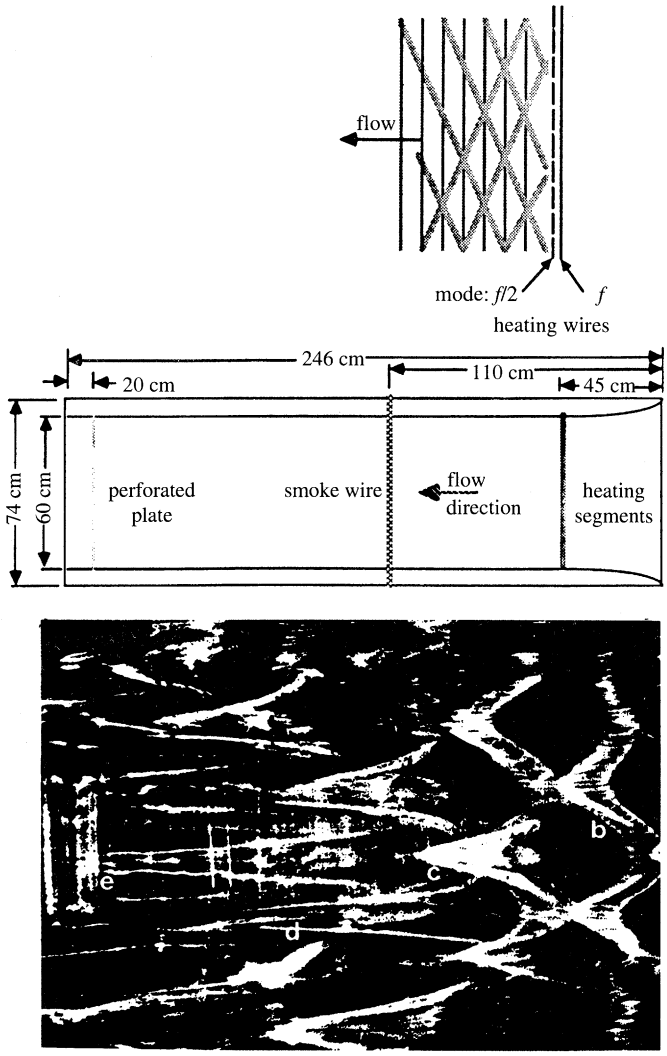

Figure 2. (Top) A schematic drawing of the wind-tunnel test section showing the location of the heating wires used for introducing periodic 2D and 3D disturbances. (Bottom) sample smoke-wire flow-visualization record showing 3D structure for subharmonic resonance.

curve. The conditions of the experiment, with respect to the Blasius neutral curve, are shown in figure 3.

3. Results

Spectra which are typical of a 'tuned' subharmonic resonance are shown in figure 4 for two x-positions. These correspond to case 0 in table 1, where the physical frequencies of the plane wave and oblique wave pairs are 32 and 16 Hz, respectively. At the upstream location (top) the spectral peaks are sharp, and the background disturbances are small with respect to these. The peak at 48 Hz is due to a summing interaction between the two input modes. The downstream spectra (bottom) correspond to the x-location of energy saturation for this case. At this point, the sub-

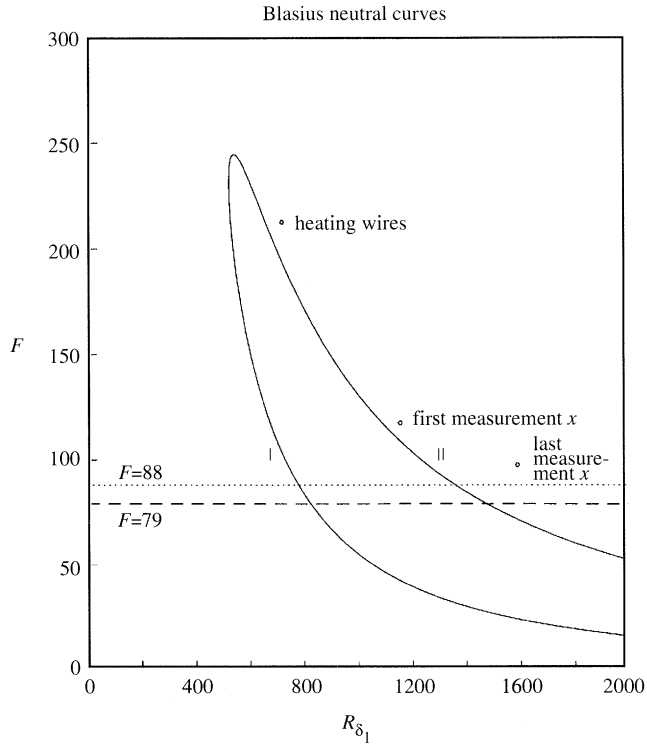

Figure 3. Positions of heating wires and measurement stations with respect to the linear stability neutral curve. Long-dotted and long-dashed lines mark the range of the 2D mode frequencies used. $F_{3D} = 39.5$.

harmonic 3D mode has grown to large amplitude and dominates the spectra. The large growth of the subharmonic mode leads to the generation of other modes due to sum and difference interactions, such as $(\frac{3}{2}f_{2D}, \frac{3}{2}\alpha_{2D}, \pm\beta_{3D})$, $(\frac{5}{2}f_{2D}, \frac{5}{2}\alpha_{2D}, \pm\beta_{3D})$, $(f_{2D}, \alpha_{2D}, \pm 2\beta_{3D})$ and $(0, 0, \pm 2\beta_{3D})$. These have all been documented by Corke & Mangano (1989). Recent measurements of our setup by Hsia (1993) have shown that the distortion of the mean profile away from Blasius typically occurs when the subharmonic mode reaches an amplitude of $u'/U_\infty \approx 5\%$. This is also the level which marks the rise in amplitude of the $(f_{2D}, \alpha_{2D}, \pm 2\beta_{3D})$. This mode is easy to distinguish from its 2D counterpart because its amplitude maximum moves away from the wall to coincide with the y-location of the subharmonic amplitude maximum. We can observe this effect by contrasting the y-distribution in amplitude for the mode at 32 Hz in the spectra at the two x-locations.

Of special interest at the downstream position of this 'tuned' case is the rise in the low-frequency (< 6 Hz) fluctuations seen in the spectra. As discussed in § 1, we believe this to be a basic characteristic which marks the later stage of subharmonic transition. Although the amplitude scale in the plot was set to show the largest peaks, we can still see that y-distribution of the low-frequency amplitude is similar to that of the subharmonic mode.

Sample spectra for a 'detuned' subharmonic resonance are shown in figure 5. These correspond to case 4, where the physical frequencies of the input plane wave and oblique wave pairs are 36 and 16 Hz, respectively. The spectra are shown at two

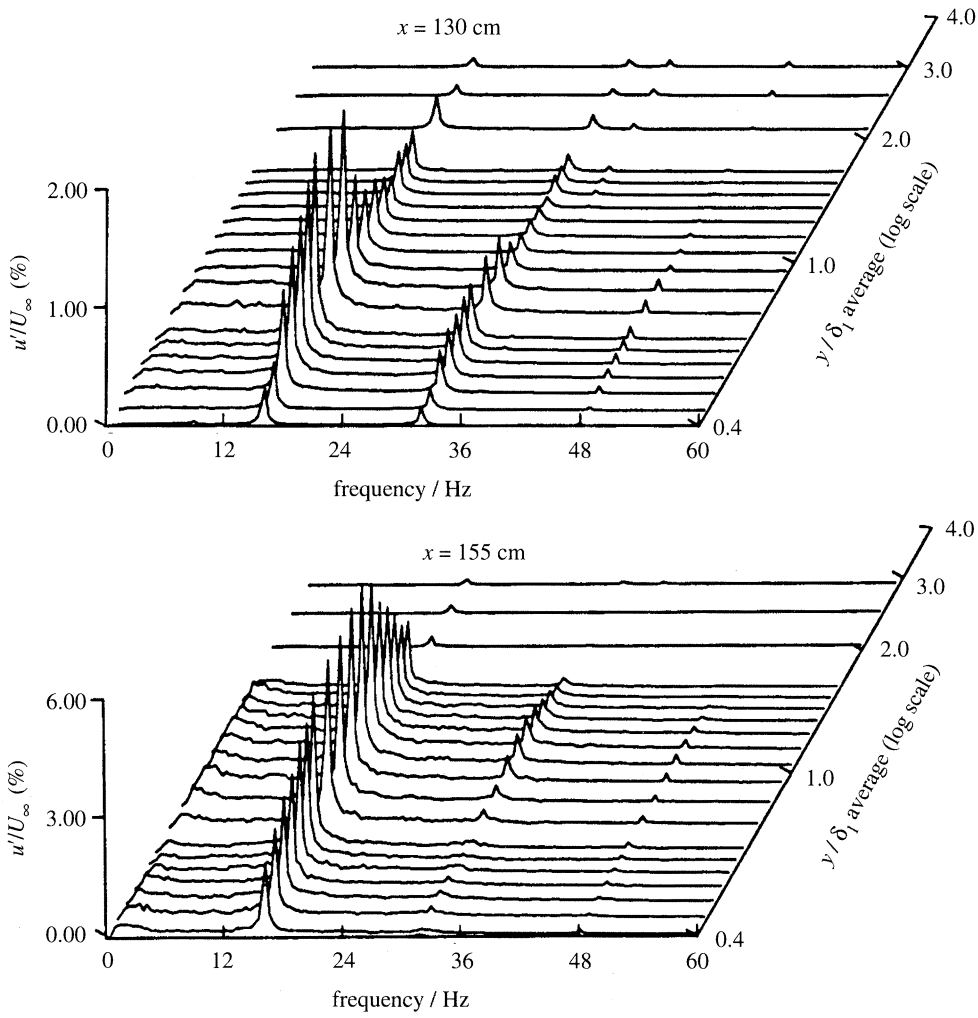

Figure 4. u-velocity spectra at different heights in the boundary layer for 16:32 tuned resonance at two streamwise locations of $x = 130$ cm (top) and $x = 155$ cm (bottom).

x-locations corresponding to the most upstream measured (top), and near energy saturation of the 16 Hz mode (bottom).

At the most upstream location, in addition to the spectral peaks at the two input frequencies, we observe other peaks at frequencies of 4, 20, 32 and 48 Hz. What is the origin of these peaks? To answer this we consider the differences between the 'tuned' and 'detuned' subharmonic resonance, which are illustrated in figure 6. Figure 6 depicts the requirements for a resonant triad between a plane wave and pairs of oblique waves with equal–opposite wave angles. These are represented in the frequency-spanwise wavenumber $(f-\beta)$ plane. For a tuned resonance (top), only *one pair* of oblique waves at $\frac{1}{2}f$ are necessary to form a triad with a plane wave at f. If, as in our detuned experiment, the frequency of the plane wave is shifted from f to $f+\Delta f$, the original pair of oblique waves at $\frac{1}{2}f$ is not sufficient to form a triad by itself. Rather, a *second pair* with the same spanwise wave number with a frequency of $\frac{1}{2}f+\Delta f$ is also needed.

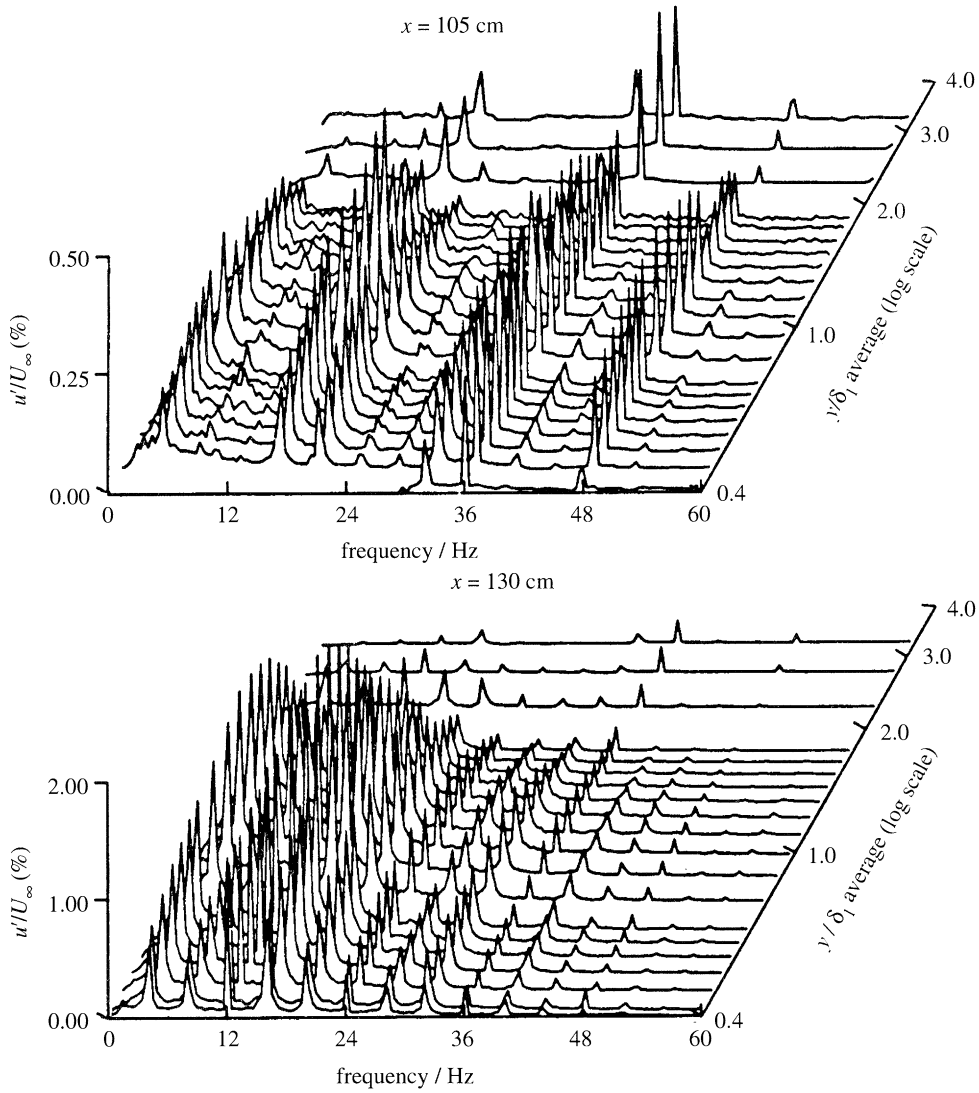

Figure 5. u-velocity spectra at different heights in the boundary layer for 16:36 detuned resonance at two streamwise locations of $x = 105$ cm (top) and $x = 130$ cm (bottom).

Looking back at the spectra in figure 5, the peak at 20 Hz corresponds to the second pair of oblique wave pairs needed for the triad resonance. It is generated by a difference interaction between the input modes: $(36, \alpha_{2D}, 0) - (16, \alpha_{3D}, \pm\beta) = (20, [\alpha_{2D} - \alpha_{3D}], \pm\beta)$. A difference interaction between the two pairs of oblique modes generates the lowest difference mode at 4 Hz, namely, $(20, [\alpha_{2D} - \alpha_{3D}], \pm\beta) - (16, \alpha_{3D}, \pm\beta) = (4, [\alpha_{2D} - 2\alpha_{3D}], \pm 2\beta)$. The other peaks in the spectrum at 32 and 48 Hz are harmonics of the input 16 Hz 3D mode.

Inherent in this view is that the initial modes at 16 and 36 Hz have the same phase speed. This is verified in figure 7, where the streamwise phase development, $\phi(x)$, multiplied by the ratio of the mode frequency to the 16 Hz frequency (f/f_{16}) is shown. For the 16 Hz mode, the slope of a line through the points gives the streamwise wave number, α_r. The phase speed is $C_r = 2\pi f/\alpha_r$. For the 36 Hz mode to have the same

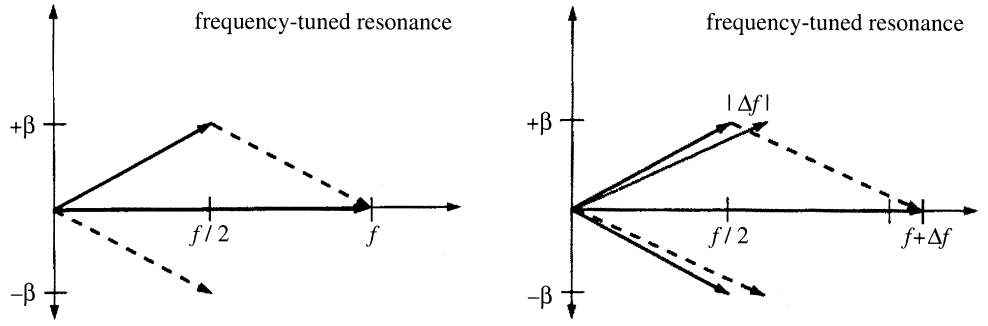

Figure 6. Schematic representation showing the frequency-spanwise wavenumber requirements for tuned (top) and detuned (bottom) triad resonance.

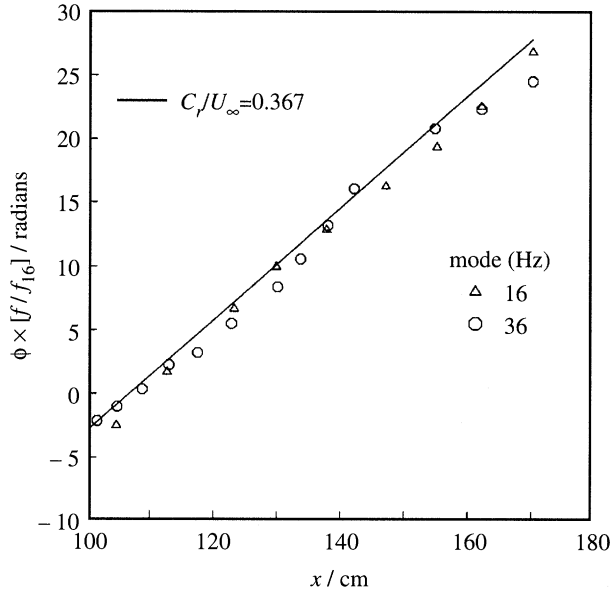

Figure 7. Streamwise phase development of the 16 and 36 Hz modes used for input in the frequency-detuned resonance case.

phase speed, the ratio of the phase slopes ($\alpha_{r_{36}}/\alpha_{r_{16}}$) should be equal to the ratio of their frequencies (36/16). Therefore, normalizing the phase in this way should produce the same slope for the two modes if they have the same phase speed. The results verify that this is the case. Drawn for reference is a line corresponding to a phase speed of $C_r/U_\infty = 0.367$, which is the value predicted from calculations.

We expect the two pairs of oblique modes (16 and 20 Hz) to grow at the same rate. In our case, because the 16 Hz mode was directly input, it will initially have a higher amplitude than the 20 Hz mode. The energy exchange between them, however, will eventually cause their amplitudes to become the same. We present evidence of this in figure 8. Shown there are the streamwise development of the maximum amplitude ($u'_{\max}/U_\infty\%$) for the modes seen as spectral peaks in figure 5. The top part of the figure shows the amplitude development for the modes which make up the triad, namely, the 2D mode (36 Hz) and two pairs of oblique modes at 16 Hz (input) and 20 Hz. As expected, the 16 Hz oblique modes start out at a higher amplitude, but

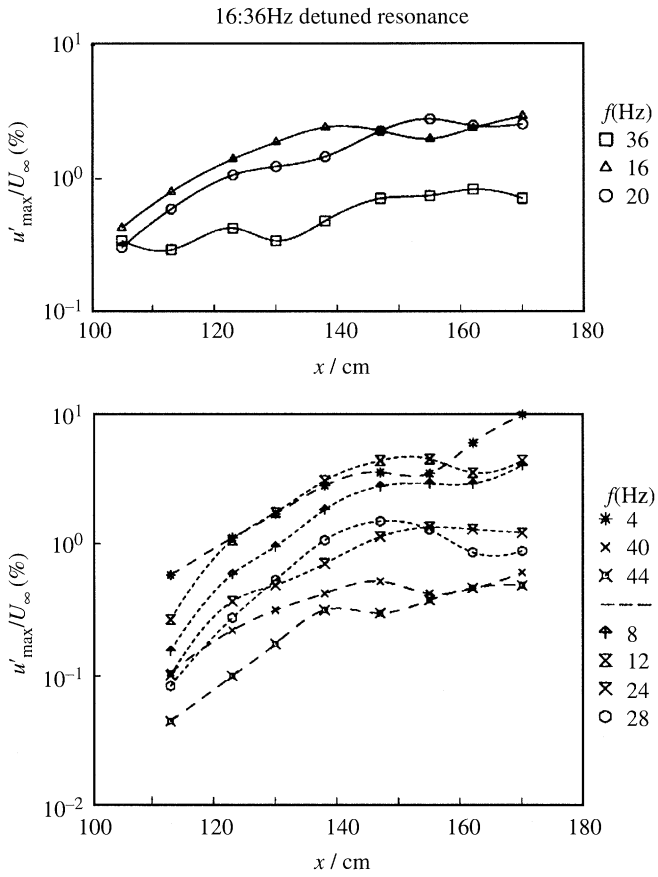

Figure 8. Streamwise development of input and nonlinearly generated modes with 16:36 Hz detuned resonance.

eventually the 20 Hz pair catches up. The amplitude undulations that occur between these two modes further downstream is characteristic of a parametric interaction.

We verify that these two modes have the same amplitude shape in figure 9, which shows a plot of the u'-amplitude distributions in the wall-normal direction for the 16 and 20 Hz modes at $x = 130$ cm. These were taken as the spectral peak values at their respective frequencies from figure 5. When these are normalized by their maximum values they collapse well onto a single distribution. The curve in the figure corresponds to the normalized profile for the subharmonic mode for a 'tuned' resonance with the same oblique mode conditions taken from Corke & Mangano (1989, figure 20, $x = 115$ cm). Also included is the distribution for the subharmonic mode from Kachanov & Levchenko (1984). Herbert (1989) found excellent agreement with this profile in his secondary instability analysis. The comparison between all of these is quite good.

In terms of the 36 Hz 2D mode, branch II from linear theory is located at $x = 130$ cm. In this case, by that location, the amplitudes of the pairs of oblique modes are large enough that the development of the plane mode is affected. The initial decrease in amplitude is due to the parametric interaction with the oblique modes. The increase in amplitude further downstream is due to the growth of energy at 36 Hz produced by a back interaction from the oblique modes.

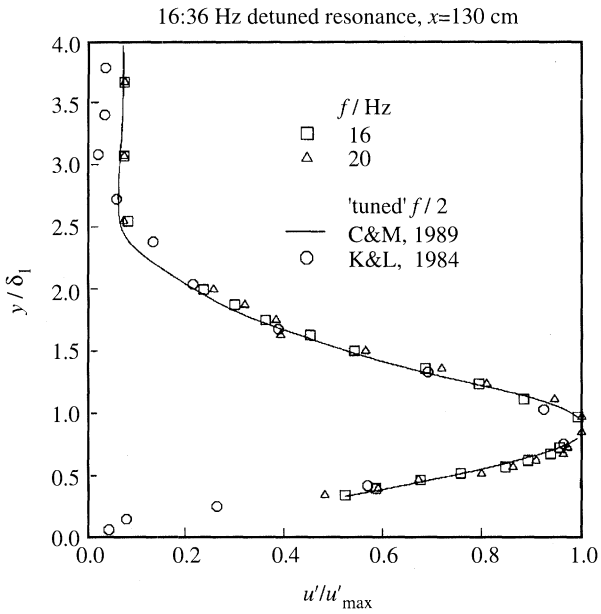

Figure 9. Amplitude profiles in the wall-normal direction for two pairs of oblique modes in 16:36 Hz detuned resonance. The curve corresponds to the amplitude profile for the subharmonic mode in the tuned case of Corke & Mangano (1989).

Table 2. *Maximum dimensionless amplification rates for* 16 : 36 Hz *detuned resonance*

f (Hz)	$\mathcal{A}_{\max}\delta_1$	f (Hz)	$\mathcal{A}_{\max}\delta_1$	f (Hz)	$\mathcal{A}_{\max}\delta_1$
36	0.007	4	0.021	8	0.030
16	0.017	40	0.019	12	0.044
20	0.015	44	0.020	24	0.032
				28	0.027

Note that $\delta_1 = 3.0$ mm.

As a result of the detuned triad resonance, there is the generation of a broad range of discrete modes in intervals of the lowest difference frequency (4 Hz in this case). The streamwise development of their maximum amplitude is presented in the bottom part of figure 8. Here we have attempted to categorize these by the order of the interaction. For example, the first group is made up of those modes that arise from a sum or difference interaction with the triad modes. These are 4 and 40 Hz. The next group comes from interactions that involve the previous group. These are 8, 12, 24 and 28 Hz. We expect that the amplification rate will increase with the group order. Looking at the slopes of the amplitude growth shows that this is generally the case. Table 2 lists the maximum dimensionless amplification rate $\mathcal{A}_{\max}\delta_1$ for all the modes in figure 8. These are based on the maximum local slope, $\mathrm{d}u'_{\max}/\mathrm{d}x$.

By order of interaction, the mode at 44 Hz should fall in the group with the 8 Hz mode, but its maximum amplification rate seems to place it in the middle group with the 4 Hz mode. Other than this one frequency, the amplification rates consistently increase with the interaction order. This provides the mechanism for

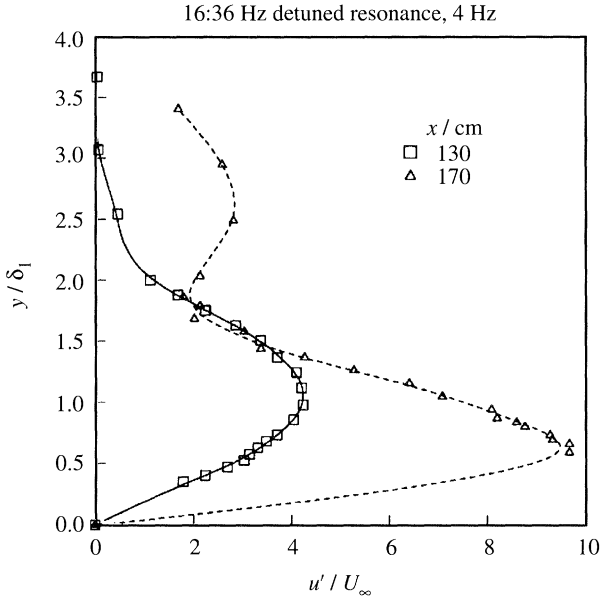

Figure 10. Amplitude profiles in the wall-normal direction for the 4 Hz mode upstream of the energy saturation ($x = 130$ cm), and in the growth region which follows further downstream ($x = 170$ cm).

the rapid growth of energy at a broad band of frequencies that can occur through a detuned subharmonic resonance, and thereby provides the questioned (?) path shown in the left flow chart in figure 1.

In terms of maximum amplitudes, the most dominant modes further downstream are those at the lower frequencies, i.e. 4, 8 and 12 Hz. This is significant because these frequencies are entering a Reynolds-number regime where they are also linearly unstable. As a result, they can grow on their own past where the triad-modes amplitudes have saturated.

The 4 Hz mode in figure 8 shows signs of a change over to linear growth by its initial amplitude saturation followed by large exponential growth past $x = 150$ cm. The wall normal u'-amplitude profiles upstream and downstream of this x-location for the 4 Hz mode, shown in figure 10, support this view. At the upstream location ($x = 130$ cm) the profile is similar to the 16 and 20 Hz modes from which the 4 Hz mode was derived. However, downstream at $x = 170$ cm, the profile has a definite linear (TS) character. This is strong evidence that further downstream, the growth in amplitude of the 4 Hz mode is due to its linear instability. We have also found that, by the last x-location, the amplitude profiles for the 8 and 12 Hz modes (not shown) also take on a TS-like character, which would account for their growth past initial amplitude saturation as well.

We have attempted to obtain a quantitative sense of the degree to which the 'detuned' subharmonic resonance will occur. To achieve this we have performed a series of experiments where we input a 3D mode pair at a fixed initial amplitude, and measure any change in amplitude at a fixed downstream location due to changing the initial amplitude of the 2D mode. The measurement location is $x = 138$ cm, which is in the middle range of the x-locations in figure 8, and just downstream of branch II. The frequency and wave angles of the 3D mode are kept fixed. The frequency of the 2D mode is changed to give different percentages of detuning, according to table 1.

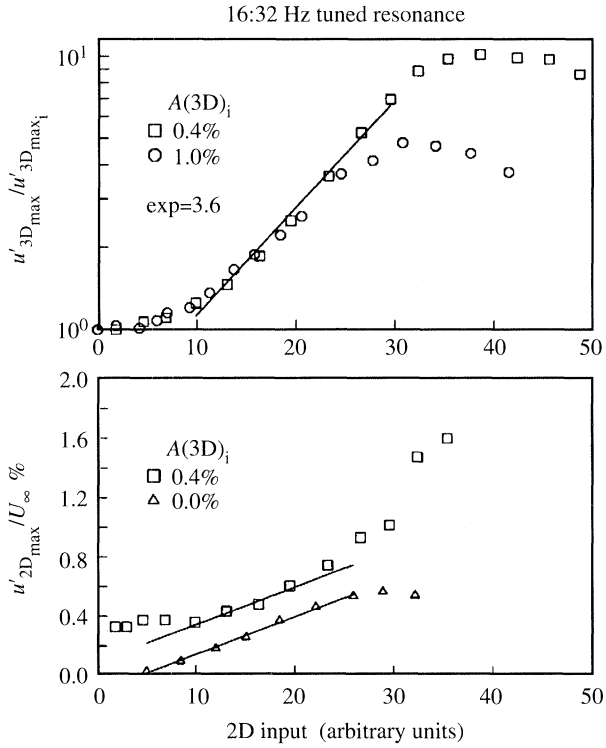

Figure 11. The effect of 2D (bottom) and 3D (top) velocity fluctuation amplitudes due to changes in input 2D forcing amplitude ($x = 138$ cm). Different symbols correspond to different initial 3D mode amplitudes.

Example results for the 16:32 Hz 'tuned' cases are shown in figure 11. The abscissa corresponds to a measure of the forcing level supplied to the 2D mode heating wire. In the bottom graph of the figure, the ordinate corresponds to the maximum amplitude of the 2D mode u-velocity fluctuations measured at $x = 130$ cm. In this case, the ordinate is on a linear scale to highlight the linear input–output relation between the forcing and 2D mode amplitudes. The two data sets correspond to different initial amplitudes of the 3D mode (16 Hz), again measured in terms of the maximum $u'/U_\infty\%$ at $x = 130$ cm, with no input 2D mode.

The ordinate in the top graph of figure 11 corresponds to the maximum amplitude of the input 3D mode. The amplitudes in this case have been normalized by their initial value (when $u'_{2D_{max}} = 0$). Here the ordinate is a log scale, in order to highlight the exponential response of the amplitude of the 3D mode due to a linear change in the amplitude of the 2D mode, which is expected to occur with resonance. The two data sets also correspond to different initial 3D amplitudes. The solid line corresponds to an exponential fit to a region of the data for the lower initial amplitude (0.4%). The corresponding exponent is given in the label on the figure.

In plots like these, we look for three characteristics: (i) an exponential growth region (signifying resonance) along with the exponent value; (ii) the 2D threshold amplitude required for resonance; and (iii) the saturation (maximum) amplitude. For the 'tuned' case at the two initial amplitudes, we observe a clear exponential growth region. In addition, the value of the exponent is independent of the 3D initial amplitude. Considering a simple three-wave resonance, the amplitude of either of the

pair of oblique (3D) modes should depend on the initial amplitude of the 2D mode by the following relation (see, for example, Corke & Kusek 1993):

$$A_{3D} = A_{3D_i} \exp(\alpha_{i_{3D}} x + A_{2D}). \tag{3.1}$$

If there is no back-interaction of the 3D mode to the 2D (simply parametric), the 2D mode amplitude is given by linear theory:

$$A_{2D} = A_{2D_i} \exp(\alpha_{i_{2D}} x), \tag{3.2}$$

so that

$$A_{3D} = A_{3D_i} \exp[\alpha_{i_{3D}} x + A_{2D_i} \exp(\alpha_{i_{2D}} x)]. \tag{3.3}$$

In this relation, for a fixed x, the amplitude of the 3D mode should vary as the exponential of the 2D mode amplitude. Further, the exponent value should be fixed for fixed linear amplification rates.

The bottom graph of figure 11 verifies that the initial portion of the 2D mode amplitude has a linear input–output relation, and that the slope is independent of 3D initial amplitude. To substantiate the latter, the same line that was fit to the data with no input 3D amplitude (triangles) was simply translated into the region of the data points for $A_{3D_i} = 0.4\%$. The reason for the apparently higher 2D amplitude when a 3D disturbance was input is that, with our setup, when introducing disturbances to excite oblique modes at 16 Hz, a small harmonic at 32 Hz is also produced. In this experiment, the oblique modes introduced at 16 Hz have wave angles of $\pm 59.6°$, which gives the largest parametric amplification rate (Corke & Mangano 1989, figure 19; Herbert & Bertolotti 1985). The harmonic excited by our 3D mode input, also consists of oblique mode pairs, but being at twice the frequency, they have smaller wave angles of $\pm 40.5°$. From single spatial-point measurements, we cannot distinguish this mode from the 2D at the same frequency. It only becomes distinguishable by the linear amplitude variation we measure once the 2D mode amplitude exceeds that of the harmonic.

In the top graph of figure 11, the growth of the 16 Hz 3D mode with $A_{3D_i} = 0.4\%$ is the companion with the 2D amplitude in the bottom graph of the figure. The exponential growth in that case is the same as that at the higher initial 3D amplitude, as we expect from equation (3.3) for a 'tuned' parametric resonance.

As the amplitude of the 3D mode grows large, we observe two effects. The first, is the growth of energy at the fundamental frequency. In the bottom graph of the figure, this is observed as the rise in amplitude, above the linear relation, for the case with $A_{3D_i} = 0.4\%$ (square symbols). Corke & Mangano (1989) have verified that this is due to a summing interaction of the subharmonic 3D mode with itself, to produce the 3D mode at the fundamental frequency $(f_{2D}, \alpha_{2D}, \pm 2\beta_{3D})$.

The second effect is the amplitude saturation of the 3D mode. This is the result of a self-interaction mechanism which is well modelled as A_{3D}^3. Since it depends on the 3D mode amplitude, it is not surprising to find that the saturation amplitude depends on A_{3D_i}. The method of normalizing by the initial amplitude in figure 11 is, however, slightly deceptive in comparing the saturation amplitudes in these two cases. In reality they are not greatly different, being 4.9% and 4.6% for $A_{3D_i} = 1.0$ and 0.4%, respectively.

How do these characteristics change with detuning? As pointed out earlier, with frequency detuning, resonance requires two pairs of oblique modes. Following our earlier experiment (Koratagere 1990), Mankbadi (1993) developed a coupled amplitude model for frequency-detuned subharmonic resonance in a Blasius boundary

layer. A general simplified form of this is

$$\frac{\mathrm{d}|A|}{|A|\,\mathrm{d}R} = C_0 + C_1\frac{|B_+|^2}{|A|} + C_3\frac{|B_-|^2}{|A|}, \tag{3.4}$$

$$\frac{\mathrm{d}|B_+|}{|B_+|\,\mathrm{d}R} = C_4 - C_5|A|\frac{|B_-|}{|B_+|} + C_6(|B_+|^2 + |B_-|^2 + C_7|B_+||B_-|), \tag{3.5}$$

$$\frac{\mathrm{d}|B_-|}{|B_-|\,\mathrm{d}R} = C_8 - C_9|A|\frac{|B_+|}{|B_-|} + C_{10}(|B_+|^2 + |B_-|^2 + C_{11}|B_+||B_-|), \tag{3.6}$$

where A refers to $A_{2\mathrm{D}}$, B_+ refers to our input 3D mode at the near subharmonic frequency with amplitude $A_{3\mathrm{D}}$, and B_- refers to the amplitude of the second pair of oblique modes needed for resonance. $C_0, \ldots, C_{11}$ are constants, which in Mankbadi's formulation depend on Reynolds number ($Re = \sqrt{Ux/\nu}$), initial phase difference and oblique wave angles.

In the notation expressed here, C_0, C_4 and C_8 represent linear amplification rates for the respective modes. When combined, this model holds the same basic structure as equation (3.3) if, with a 'tuned' case, B_+ and B_- are replaced by the single amplitude B, and the cubic interactions for B and the back interaction of B on A are neglected.

Focusing on the quadratic terms in equations (3.5) and (3.6), with 'detuning', the parametric growth rate of the detuned input oblique modes is coupled with the growth rate of the second pair. This drives the two pairs towards the same amplitude as was documented at the top of figure 8. In addition, contrary to the 'tuned' case, the parametric growth rate of the input oblique modes B_+ will depend on its initial amplitude through the coupling with B_-.

As pointed out for the 'tuned' case, the cubic amplitude term results in the saturation of the parametric growth. In Mankbadi's (1993) model for a 'detuned' resonance, the cubic interaction is significantly stronger because, in addition to the self-interaction which occurs in the 'tuned' case, it also involves a cross-interaction between each pair of oblique modes.

We have investigated these properties in a series of experiments similar to those presented for the 'tuned' cases in figure 11. Specifically, we have examined the effect of 3D mode initial amplitude and percentages of subharmonic frequency detuning on the parametric growth rate, saturation amplitude and 2D threshold amplitude. Figure 12 documents the effect of the initial 3D amplitude for the largest amount of detuning examined (12%, case 4 in table 1). The presentation is similar to the top part of figure 11, except that the abscissa has been directly converted into the equivalent 2D mode velocity fluctuation $u'_{2\mathrm{D}_{\max}}/U_\infty\%$, and the 3D mode amplitude on the ordinate is normalized by U_∞ rather than by its initial value. The 3D mode in this case refers to the input mode which is always at 16 Hz. Also, the 2D mode amplitude was measured without a 3D mode input, and was verified to be linear over this range.

The initial amplitude levels of the four cases in figure 12 were nominally $u'_{3\mathrm{D}_{\max}}/U_\infty = 0.1$, 0.2, 0.4 and 0.7%. In all four cases we have verified a region of exponential growth of the 3D mode, signifying resonance. This is shown by the straight line which was fitted to that portion of the data. The exponent values are listed in the label on the figure.

The results in this figure are in concurrence with the model equation predictions. In particular, we observe an increase in the parametric growth rate (exponent) with

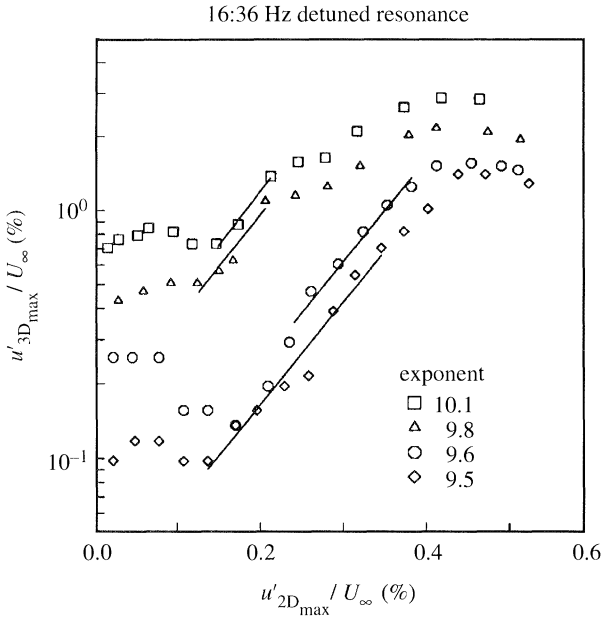

Figure 12. The effect of the initial 3D amplitude on the nonlinear response of the 3D mode to the 2D initial amplitude ($x = 138$ cm).

an increasing 3D initial amplitude. The extent of the exponential growth, however, decreases significantly with increasing 3D amplitude, which is consistent with the extra-strong cubic interaction. Compared to the 'tuned' case, there is a substantial increase in the exponent with detuning (9–10 against 3.6), and a substantial decrease in the saturation amplitude ($\leqslant 2.8\%$ against $\geqslant 4.8\%$).

At a fixed 3D initial amplitude of 0.7%, figure 13 documents the effect of the amount of detuning on these characteristics. Here we emphasize again that the detuning was achieved by changing only the 2D mode frequency. The frequency combinations and their corresponding symbols are listed in the figure label. Even though the change in the 2D frequency is small, there is a slight change in the linear amplification. In making a comparison between these cases, we have accounted for this effect.

In each case, we can identify an exponential growth region. As before, the exponential fit is shown by the solid line and the exponent value is given in the label. Here we observe an increase in the exponent with increasing frequency detuning. The 16:33 Hz detuned case has the same exponent value as the 'tuned' case.

Even the smallest amount of detuning (3.1%) gives a significant drop in the saturation amplitude. A further increase in the percentage of frequency detuning lowers the maximum amplitude, but with a lesser effect.

Finally, we observe a decrease in the threshold amplitude of the 2D mode before 3D exponential growth with increasing detuning. We determine this value by the point of intersection of the extrapolation of the exponential fit (solid line) in each case to an imaginary horizontal line at the initial 3D amplitude (0.7%).

We have combined these results to produce figure 14. This shows the trends in exponent value, 2D threshold and saturation amplitude as a function of the frequency detuning. Most of the data is for $u'_{3D_{max}}/U_\infty = 0.7\%$, although isolated results for 0.4 and 1.0% are also included. A smooth curve is passed through the points which belong

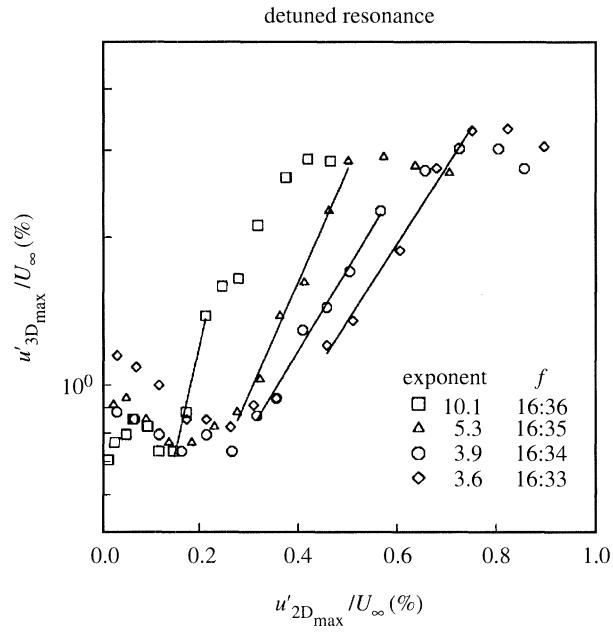

Figure 13. The effect of the detuning percentage on the nonlinear response of the 3D mode to the 2D initial amplitude ($x = 138$ cm).

to the 0.7% initial amplitude set. For the exponent, the curve includes the 'tuned' case (solid square symbol) since the parametric growth in that case is independent of the 3D initial amplitude.

For the 2D threshold amplitude, the trend of the 0.7% data appears to extrapolate well towards the value for the 'tuned' case. The results for the most detuned cases however, indicate a sensitivity to initial amplitude. The 'tuned' datum in this figure was at $u'_{3D_{max}}/U_\infty = 0.4\%$. Therefore, a proper extrapolation of the 0.7% trend should likely bring it slightly above the 0.4% threshold level.

In terms of the saturation amplitude, figure 14 reiterates that a significant reduction in the maximum amplitude occurs with only a small amount of detuning. For a given detuning percentage, the actual reduction also depends on the 3D initial amplitude. As seen in the figure, the sensitivity to initial amplitude is largest at the higher detuning amounts.

4. Discussion and conclusions

As stated in § 1, our objective in studying 'detuned' subharmonic resonance was to investigate a mechanism for the generation of a broadband spectrum from an initial spectrum with only a few discrete modes. This was motivated by our previous experiments (Corke & Mangano 1989; Corke 1989) which indicated that transition, starting from an exact fundamental/subharmonic resonance, eventually developed energy side-bands which were then involved in successive sum and difference interactions to rapidly generate a broad spectrum. Of special significance in this process was the growth of energy in the lowest band of frequencies, which could account for the low-frequency amplitude modulation seen by Kachanov & Levchenko (1984). The appearance of the side-bands also closely coincided with subharmonic amplitude saturation.

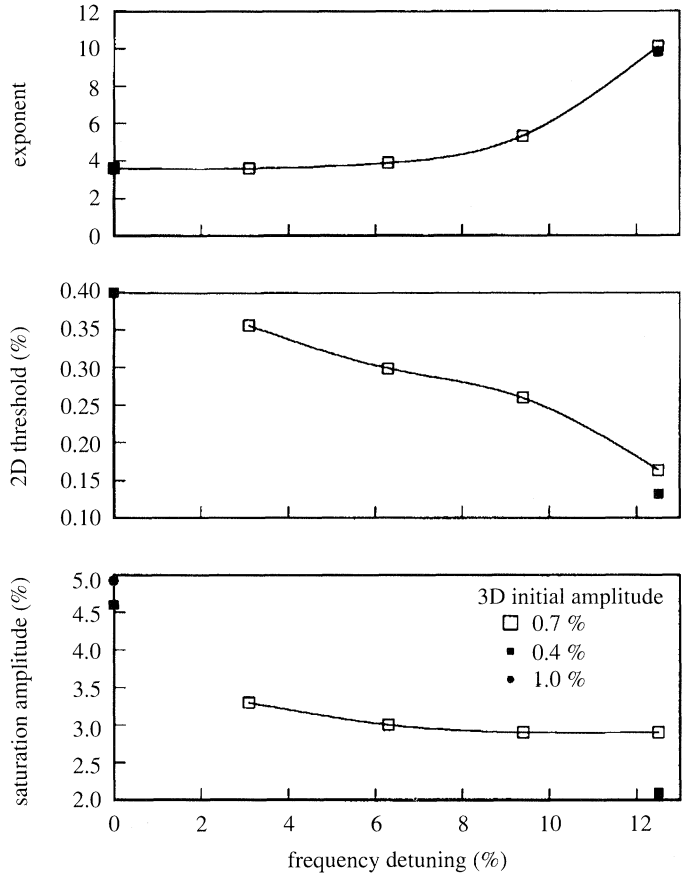

Figure 14. The variation of parametric exponent, 2D threshold and saturation amplitude with frequency detuning percentage. Different symbols correspond to different initial 3D mode amplitudes.

The question we then tried to answer was, starting from an initially 'tuned' resonance, is there a tendency for this process to 'detune'? If so, can it account for the rapid growth of the broadband spectrum, including very low frequencies, and is it important in limiting the maximum amplitude of the subharmonic mode?

Based on the results presented here, the answer is *yes*. However, more importantly, they suggest that, except under well controlled laboratory conditions, the most likely subharmonic transition will be '*detuned*' *from the onset*. This scenario corresponds to the flow chart on the right-hand side of figure 1. The support for this comes from our results which indicate that with frequency detuning:

(i) there is a reduction in the 2D threshold amplitude needed for 3D mode resonance;

(ii) there is an increase in the parametric growth rate; and

(iii) the parametric growth rate increases with 3D mode initial amplitude.

The implications are that with uncontrolled stochastic disturbance input, which is more relevant to natural transition situations, a 'detuned' subharmonic resonance would likely be the first to occur.

At whatever stage detuning occurs, the additional modes that are generated by sum and difference interactions are highly amplified and rapidly fill the spectrum.

In addition, energy in the lowest frequencies, initially fed by nonlinear interactions, can be later amplified by linear mechanisms so that they may ultimately be most dominant at the later stages of transition.

The overall growth of the initial 3D mode is determined by the combination of the parametric growth rate and cubic interaction. With detuning, the larger initial growth is more than offset by the extra-strong saturation mechanism, so that compared to a 'tuned' case, the total growth is less. Therefore, transition prediction schemes based on following a path of largest total 3D mode growth could give misleading results if conditions favour detuning.

Finally, with larger detuning amounts, the larger parametric growth rates, and reduced 2D threshold documented in our results, make the development of the 3D triad modes especially sensitive to the 2D amplitude. For example, even small spanwise variations in the 2D mode initial amplitude could lead to significantly different 3D amplitudes downstream. The result would be a jagged transition front which largely mimics the 2D initial condition.

The author is indebted to Srinivassan Koratagere for his dedicated work in the laboratory compiling the data presented here. The interpretations of this work has benefited from frequent discussions with Dr Reda Mankbadi. This work was supported by the U. S. Air Force Office of Scientific Research Grant 90-0173.

References

Corke, T. C. & Mangano, R. A. 1989 Resonant growth of three-dimensional modes in transitioning Blasius boundary layers. *J. Fluid Mech.* **50**, 93.

Corke, T. C. 1989 Resonant three-dimensional boundary layers—structure and control. AIAA shear flow control conference, AIAA-89-1001.

Corke, T. C. 1990 Effect of controlled resonant interactions and mode detuning on turbulent transition in boundary layers. In *IUTAM Symp. on Laminar-Turbulent Transition* p. 151. Berlin: Springer.

Corke, T. C. & Kusek, S. K. 1993 Resonance in axisymmetric jets with controlled helical-mode input. *J. Fluid Mech.* **249**, 307.

Craik, A. D. D. 1971 Nonlinear resonant instability in boundary layers. *J. Fluid Mech.* **50**, 393.

Herbert, Th. 1983 Secondary Instability of plane channel flow. *Phys. Fluids* **26**, 871.

Hsia, Y.-C. 1993 Amplitude ratio effects on 3D mode resonance in boundary layers. M.Sc. thesis, Illinois Institute of Technology.

Kachanov, Yu. S. & Levchenko, V. Ya. 1984 The resonant interaction of disturbances at laminar-turbulent transition in a boundary layer. *J. Fluid Mech.* **138**, 209.

Klebanoff, P. S., Tidstrom, K. D. & Sargent, L. M. 1962 The three-dimensional nature of boundary layer instability. *J. Fluid Mech.* **12**, 112.

Koratagere, S. 1990 Broadband 3D mode development in a Blasius boundary layer by resonant mode detuning. M.Sc. thesis, Illinois Institute of Technology.

Mankbadi, R. R. 1993 The interaction of frequency-detuned modes in boundary layers. AIAA paper 93-0341.

Santos, G. R. 1987 Studies on secondary instabilities. Ph.D thesis, Virginia Polytechnic and State University.

Santos, G. R. & Herbert, Th. 1986 Combination resonance in boundary layers. *Bull. Am. phys. Soc.* **31**, 1718.

PHILOSOPHICAL TRANSACTIONS OF THE ROYAL SOCIETY A MATHEMATICAL, PHYSICAL & ENGINEERING SCIENCES